Journal of Sound and Vibration (1998) **215**(5), 1015–1041
Article No. sv981618

REMOTE IDENTIFICATION OF IMPACT FORCES ON LOOSELY SUPPORTED TUBES: PART 1—BASIC THEORY AND EXPERIMENTS

M. De Araújo* and J. Antunes

Instituto Tecnológico e Nuclear, Applied Dynamics Laboratory, ITN/ADL, 2686 Sacavém Codex, Portugal

and

P. Piteau

Commissariat à l'Energie Atomique, Département de Mécanique et Technologie, CEA/DMT, 91191 Gif-sur-Yvette Cedex, France

(*Received* 21 *April* 1997, *and in final form* 10 *March* 1998)

Flow-induced vibration of heat-exchanger tube bundles is an important issue, concerning component life and plant availability. Predictive methods have been developed to analyze heat-exchanger tube responses and wear, for realistic multi-supported tubes and flow configurations. Experimental validation of these methods is currently pursued by several research groups, with considerable success. However, experiments on vibro-impacting tubes involve very carefully instrumented test tubes and tube-supports, which is seldom possible in real field components, due to space limitations and severe environment conditions. Hence, there is a need for identification techniques that enable the diagnostic and field monitoring of tube-support interaction under real operating conditions, using information from motion transducers located far from the impact locations. In this paper, the basic theory for the propagation of flexural waves is briefly reviewed, and techniques are developed for the experimental identification of the wave path propagation parameters and impact forces, from tube response measurements at remote locations. These inverse problems are quite sensitive to the noise contamination of measurements. Optimization techniques are used to overcome these difficulties, and their merits are accessed using extensive numerical simulations. Then, experiments performed on a long steel beam are presented. A simple method is developed to deal with the boundary reflections of a wave generated by a single impact. Experimental identification of the wave-path properties, of isolated impact forces and also of impact locations is performed. Overall, quite good agreement was found between directly measured and remotely identified quantities.

1. INTRODUCTION

Flow-induced vibrations of heat-exchanger tube bundles are a main source of concern, when component life and plant availability are addressed. Indeed, excitation by the flow turbulence or even fluidelastic phenomena may lead to premature failure due to fatigue or vibro-impact wear between tubes and tube supports. This has been demonstrated by many experiments, as well as by field reports. The authors and other researchers have developed predictive methods and computer codes to analyze heat-exchanger tube responses and wear, for realistic multi-supported tubes and flow configurations [1–12]. Experimental validation of these methods is a large-scale enterprise, currently pursued by several research groups, with considerable success [13–19].

* Visiting student from Ecole Nationale Supérieure des Arts et Métiers (ENSAM), Paris, France.

0022–460X/98/351015 + 27 $30.00/0

However, laboratory experiments on vibro-impacting tubes usually involve very carefully instrumented test tubes and tube-supports—a luxury that is seldom possible in real field components, due to space limitations and severe environment conditions (temperature, radiation, . . .). The present authors are therefore convinced that there is an urgent need for identification techniques that enable the diagnosis of tube-support interaction under real operating conditions, using information from motion transducers (e.g., accelerometers, strain gages) located far from the impact locations. Such techniques will be valuable for validation of predictive methods, under real-life conditions, as well as for condition monitoring performed on real components. These issues will be addressed in a series of papers.

The limited work which has been published in this field will be now reviewed briefly. In two pioneering papers, Whiston [20] and Jordan and Whiston [21] discussed theoretical and experimental aspects related to the remote identification of impact forces. These authors modelled the flexural propagation waves in the frequency domain, using a Timoshenko beam model without damping. In his book, and also in a series of related papers, Doyle [22] followed a similar approach. These authors have presented experimental results which are quite satisfactory, provided by single impacts acting on long beams, in such a way that wave reflections at the boundaries do not interfere seriously with the direct wave used for identification purposes.

On the other hand, in a series of papers, Lin and Bapat [23, 24] have presented methods for estimation of the impact forces and also of the support gap for a single-degree-of-freedom system, for sinusoidal and random excitations. The extension of these methods to a beam with a single non-linear gap-support was proposed using a modal approach in the frequency-domain [25]. Also, Busby and Trujillo [26] presented a similar approach, where the force identification is achieved in the time-domain. The extension of these interesting methods to multi-supported beams with an ill-defined or unknown modal basis is far from obvious. In a recent paper, Wu and Yeh [27] discussed the problem of source separation, for several simultaneous impacts, using a time-domain approach. The so-called cepstral methods of deconvolution, which may be quite useful when dealing with non-dispersive phenomena, have been used very seldom for dispersive flexural waves [28].

Most of the basic work on inverse theory was triggered by identification problems in the geophysics/astrophysics and radar/sonar research fields. These problems usually involve non-dispersive phenomena, and lead to problems somewhat different from those which concern us. Nevertheless, for an approach to inverse problems, readers will find useful information in the applied work by Jeffrey and Rosner [29, 30], Dimri [31] and Parker [32]. In a more general context, Press *et al*. [33], Groetch [34] and Hansen [35] presented excellent reviews on inverse problems and current methods for solving them.

The main difficulty is due to ill-conditioning—physical or numerical—of the transformation (propagation) operators which describe the phenomena. This leads to inverse formulations which are very sensitive to noise contamination of the measured signals. Usually, problems are partially overcome by regularization of the transformation operators, using several methods—namely, singular value decomposition, incorporation of physical constraints and optimization techniques [33–35]. In this series of papers, we will address some of these methods, in the context of vibro-impact system identification. Ill-conditioning difficulties are enhanced for such problems, due to the dispersive nature of flexural waves.

The laboratory experiments performed by most authors usually lead to adequate estimations of the impact forces. However, their tests are based on very restrictive experimental conditions, such as: well-known system parameters, usually a single impact location and negligible noise contamination. Therefore, these experiments are very remote

from the operating conditions of real-life industry components, which emphasizes the need for further work. Earlier efforts by Whiston [20] and Doyle [22] inspired the general approach adopted in this paper. However, we discuss in detail several identification issues (regularization methods and sensitivity to noise contamination), using extensive numerical simulations. Current problem restrictions will be relaxed in future papers, in order to extend the identification methods to complex system dynamics [36].

In the first part of this paper, some basic theory for the propagation of flexural waves is reviewed. Then, techniques are developed for dealing with the following inverse problems: identification of the propagation parameters, from tube travelling wave measurements; identification of the impact forces, based on response measurements at remote locations; identification of the impact locations, using the fact that flexural waves are dispersive.

Several optimization techniques are developed to overcome ill-conditioning difficulties, and their relative merits are accessed. Also, a simple method is presented which removes the boundary reflections from the original wave generated by an isolated impact.

To conclude the paper, experimental results are presented, for a long (6 m) steel beam with non-anechoic boundaries. The properties of the wave-path are experimental identified and remote identification of isolated impacts is successfully performed. Blind estimation of the impact location is also achieved. Overall, quite good agreement was found between directly measured and remotely identified impact forces, by using simple Bernoulli–Euler beam theory for modelling wave propagation.

2. THEORETICAL FORMULATION

As discussed later, the simple Bernoulli–Euler theory for flexural vibrations—which was tentatively used in this work—proved to be adequate for impact identification. Therefore, only this basic formulation (which neglects rotational inertia and shear deformation effects) will be addressed here. Then, for a viscous damping model, the small-amplitude flexural response of a beam (with constant cross-sectional properties) is described by the differential equation (see, for instance, reference [37])

$$EI\,\partial^4 y/\partial x^4 + \rho A\,\partial^2 y/\partial t^2 - N\,\partial^2 y/\partial x^2 + \eta\,\partial y/\partial t = F(t), \tag{1}$$

where $F_y(t)$ is the external force and $y(t)$ is the dynamic vibratory response, E is Young's modulus and ρ is the mass density of the beam, A is the area and I is the moment of inertia of the cross-section, N is the axial tension of the beam and η is a viscosity coefficient. In this paper, parameters E, ρ, A, I, N and η are assumed constant along the beam. (A list of nomenclature is given in the Appendix.)

Wave solutions of equation (1) will be assumed in the form $C\,\mathrm{e}^{-\mathrm{i}(kx-\omega t)}$. With, for the moment, the axial tension and damping effects neglected, a solution of equation (1) may be obtained in the form

$$y(x,t) = \sum_n (C_{1n}\,\mathrm{e}^{-\mathrm{i}k_n x} + C_{2n}\,\mathrm{e}^{\mathrm{i}k_n x} + C_{3n}\,\mathrm{e}^{-k_n x} + C_{4n}\,\mathrm{e}^{k_n x})\,\mathrm{e}^{\mathrm{i}\omega_n t}, \tag{2}$$

where, for each circular frequency ω_n, the parameter k_n is given by the so-called dispersion relation

$$k_n = [\rho A/EI]^{1/4}\sqrt{\omega_n}, \tag{3}$$

and the parameters C_{1n} to C_{4n} are frequency dependent.

Equation (1) is said to be dispersive because the phase speed $c_n = \omega_n/k_n$ is not constant with respect to frequency. Physically, this means that travelling waves change their shape and "expand" as they propagate. From equation (3), one has $c_n \propto \omega^{1/2}$, which means that an unbounded propagation speed would be obtained as $\omega \to \infty$, an obviously unrealistic conclusion. Such problems may be conveniently dealt with by using a Timoshenko beam model. However, in practice, very high-frequency waves may not be excited and will be buried in the experimental noise—we believe these are the reasons why the simple model (1) gives adequate results.

One should notice that the first and second terms of solution (2) are propagating waves, while the third and fourth terms are non-propagation (evanescent). Physically, the two propagating terms represent a forward and a backward travelling waves. The two evanescent terms are significant only near the sources of discontinuous behaviour—such as excitation locations, changes in the wave-path cross-section and the system boundaries—and they are spatially damped outside these disturbance regions (see section 3.1). Hence, these terms are useless when identifying sources from remote-location responses, as their inversion will obviously lead to unstable results. Thus, one should be prepared to accept some errors in the identification procedure. Also, to avoid a strong influence from the near-field evanescent terms, response transducers should not be located near the beam ends. From the preceding discussion, each travelling wave in equation (2) is given by

$$y_f(x, t) \cong \sum_n C_{nf}\, \mathrm{e}^{-\mathrm{i}k_n x + \mathrm{i}\omega_n t}, \qquad y_b(x, t) \cong \sum_n C_{nb}\, \mathrm{e}^{\mathrm{i}k_n x + \mathrm{i}\omega_n t}, \tag{4}$$

where the parameters C_n depend on the initial motion conditions and also on the external excitation. Two important applications will be highlighted here.

(a) *Wave propagation in a free system*. Upon assuming, for convenience, that the beam response $y_0(t) \equiv y(0, t)$ is measured at location $x = 0$ during time T, the coefficients Y_n of the spectral form

$$y_0(t) = \sum_n Y_n\, \mathrm{e}^{\mathrm{i}\omega t} \tag{5}$$

may be computed from Fourier analysis. Then, the propagated wave can be predicted at any other location x by using

$$y_f(x, t) \cong \sum_n Y_n\, \mathrm{e}^{-\mathrm{i}k_n x + \mathrm{i}\omega_n t}, \qquad y_b(x, t) \cong \sum_n Y_n\, \mathrm{e}^{\mathrm{i}k_n x + \mathrm{i}\omega_n t}. \tag{6}$$

These equations will be used to estimate the wave-path propagation parameters, from response measurements.

(b) *Travelling wave generated by a localized force*. If a normal force $F_y(t)$ is applied at location $x = 0$ (during a time T) then, upon assuming a constant bending stiffness EI and using the spectral form

$$F_y(t) = \sum_n F_n\, \mathrm{e}^{\mathrm{i}\omega_n t}, \tag{7}$$

the beam response at location x is given by [22, 38]

$$y_f(x,t) \cong \frac{1}{4EI}\sum_n \frac{F_n}{k_n^3}\,\mathrm{i}\,\mathrm{e}^{-\mathrm{i}k_n x+\mathrm{i}\omega_n t}, \qquad y_b(x,t) \cong \frac{1}{4EI}\sum_n \frac{F_n}{k_n^3}\,\mathrm{i}\,\mathrm{e}^{\mathrm{i}k_n x+\mathrm{i}\omega_n t}, \tag{8}$$

These equations will be used to convert from the impact forces to response measurements and for force estimation.

Equations alternative to equations (6) and (8) can be easily obtained when dealing with velocity, acceleration and strain signals. If the axial tension N and damping effects are included, the dispersion relation is more complex than equation (3) and k_n will display both real and imaginary parts. Then, it is easy to show that

$$k_n = \sqrt{-\frac{N}{2EI}+\sqrt{\left(\frac{N}{2EI}\right)^2+\frac{\rho A}{EI}\,\omega^2}-\mathrm{i}\frac{\eta}{EI}\,\omega}, \tag{9}$$

and the wave-path properties depend on three parameters. When $N=0$ and the viscous damping coefficient η is small, k_n may be approximated by

$$k_n = \mathscr{C}\sqrt{\omega_n}-\mathrm{i}\mathscr{D}\frac{1}{\sqrt{\omega_n}}, \tag{10}$$

with $\mathscr{C}=[\rho A/EI]^{1/4}$ and $\mathscr{D}=(\eta/4\rho A)\mathscr{C}$. Often, the propagation environment is such that the damping coefficient is frequency dependent, a difficulty which has been discussed by Morse and Ingard [37]. For the low-damped beams considered in this work such effect was found negligible, as shown in our experimental results.

Another plausible model for damping phenomena, based on complex beam stiffness, would lead to the simpler formulation

$$k_n = (\mathscr{C}-\mathrm{i}\mathscr{D}')\sqrt{\omega_n}, \tag{11}$$

where $\mathscr{D}'$ is a suitable loss factor. This hysteretic damping model leads to non-causal responses when used with impulsively excited systems [39]. However, such a conceptual problem was found negligible, for lightly damped beams.

It should be noted that the preceding formulation, which will be used in the next sections, applies only when the non-linear effects arise from a few spaced impact stops. Such is the case addressed in the present paper, where a system with a single gap-support is analyzed. However, when systems display a large number of impact elements—or even distributed limiters—wave propagation is significantly affected by the spatial distribution of non-linear boundary conditions. These aspects have been thoroughly discussed by Babitsky and Krupenin [40] and Krupenin and Veprik [41], as well as in their referenced work. Under such conditions, the simple Bernoulli–Euler dispersion relation should not be used.

In practice, manipulation of the preceding formulations can be conveniently achieved by fast Fourier transforming all the time-domain signals. Then propagation in the frequency domain are given by simple products of functions. Finally, the time-domain estimated results are obtained by inverse Fourier transforms. For instance, the forward waves from equations (6) and (8) are computed as

$$Y_n = \mathscr{F}[\,y_0(t)] \quad \text{and} \quad G_{fn}(x) = \mathrm{e}^{-\mathrm{i}k_n x} \rightarrow Y_{fn}(x) = Y_n G_{fn}(x) \rightarrow y_f(x,t) = \mathscr{F}^{-1}[Y_{fn}(x)],$$

and

$$F_n = \mathscr{F}[F(t)] \quad \text{and} \quad \tilde{G}_{fn}(x) = \frac{\mathrm{i}}{4EIk_n^3}\,\mathrm{e}^{-\mathrm{i}k_n x} \rightarrow Y_{fn}(x) = F_n \tilde{G}_{fn}(x) \rightarrow y_f(x,t) = \mathscr{F}^{-1}[Y_{fn}(x)].$$

The same reasoning applies for computing backward waves and also for inverse problems. The properties of direct and inverse Fourier transforms, as well as their existence conditions, have been discussed by Titchmarsh [42] and Sneddon [43]. In the context of this work, all signals of practical interest are forward- and back-transformed without difficulties. Obviously, some care is needed when choosing the processing time block T, in order to encompass fully the propagated waves (some very low frequency wave responses will be always truncated). Due to the finite time-window of discrete Fourier transforms, signals become artifically periodic (wraparound with period T) after processing in the frequency domain. This induces spurious effects at the beginning and at the end of the processed time-window, which are enhanced when transients arise in these regions. Typically, to mitigate this problem, the time-data is multiplied by a suitable weighting window [44]. However, this also introduces distortions in the signals, something to be avoided for identification purposes. Therefore, the approach used in this work was to process the data by using a slightly longer time-window than displayed. From our experience, dropping the initial and last 5% of the processed signals is enough to disguise the artefacts which stem from finite-length time-windows. On the other hand, the sampling rate $1/\Delta t$ must be higher than twice the Nyquist frequency to avoid aliasing effects—see, for instance, reference [44] or[45]. Signal filtering is also an important issue, which will be addressed in Part 2 of this work, because no filtering was performed on the data of the present paper.

3. IDENTIFICATION PROCEDURES

3.1. INVERSION DIFFICULTIES

An infinite beam model is used for all the numerical simulations presented in this paper. The displacement wave pulse $y_0(t)$, shown in Figure 1(a), is generated at location $x = 0$. The simple relation (11) was used as a propagation model, with parameters $\mathscr{C} = 0{\cdot}3446$ and $\mathscr{D}' = 0{\cdot}002$—these are plausible values, however, $\mathscr{D}'$ is higher than expected for a metal beam in air (see section 4.4). This value was chosen to emphasize the role of damping in the identification procedure. Time histories are computed by using 16 384 data values with a sampling rate $\Delta t = 10^{-6}$ s. Figures 1(b–f) clearly show the wave dispersion effect, when responses $y_f(x, t)$ are computed at locations $x = 0{\cdot}05$, $0{\cdot}2$, $0{\cdot}5$, 1 and 2 m. Also, the superposed undamped waves (computed by using $\mathscr{D}' = 0$) show that damping effects are significant when $x > 1$ m. One can notice that the wave response at location $x = 0{\cdot}05$ m appears to be non-casual. This results from the propagation model (4), which was used in this simulation instead of the full formulation (2). Hence, the non-casual wave distortion displayed by Figure 1(b), which is negligible at more remote locations, when the evanescent terms become irrelevant.

Figures 2(a–d) show some estimations of the original wave pulse $y_0(t)$, obtained by inversion,

$$Y_0(\omega) = Y_f(x, \omega)/G_f(x, \omega), \tag{12}$$

of noisy "measurements" $y_f(x, t)$ (at location $x = 1$ m), for several levels of the noise-to-signal contamination (0, 10, 20 and 50%)—these percentages are defined by using the r.m.s. levels of white-noise contamination, with respect to the r.m.s. value of each wave signal. Here, the wave-to-wave transfer function G_f was first computed by using the true values of $\mathscr{C}$ and $\mathscr{D}'$ (intermediate plots), and then neglecting damping effects, $\mathscr{D}' = 0$ (lower plots). Results show that this identification problem is well-posed, provided one neglects damping effects when inverting the remote wave. Indeed, normal (positive) damping for

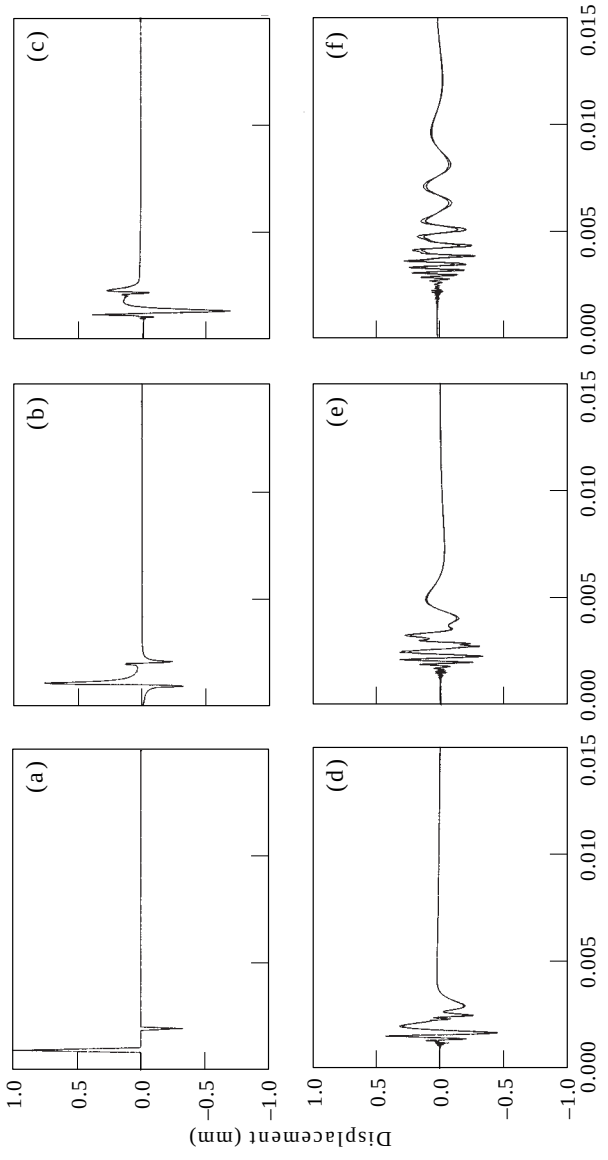

Figure 1. Typical propagation of a flexural wave (generated with $\mathscr{C} = 0{\cdot}3446$ and $\mathscr{D}' = 0{\cdot}002$) in an infinite beam: (a) $x = 0$ m; (b) $x = 0{\cdot}05$ m; (c) $x = 0{\cdot}02$ m; (d) $x = 0{\cdot}5$ m; (e) $x = 1$ m; (f) $x = 2$ m.

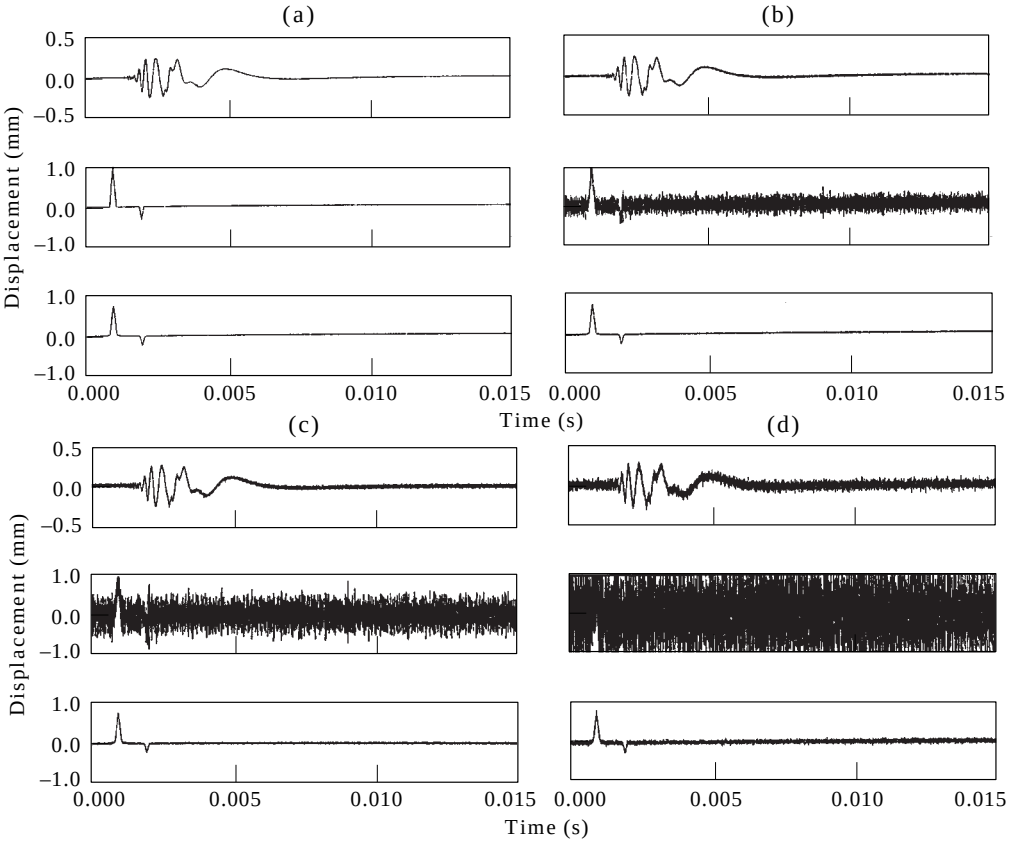

Figure 2. Identification of a remote displacement, from the travelling wave (generated with $\mathscr{C} = 0{\cdot}3446$ and $\mathscr{D}' = 0{\cdot}002$) measured at distance $x = 1$ m. Effect of the noise contamination: (a) 0% noise; (b) 10% noise; (c) 20% noise; (d) 50% noise. In each part: top, noisy wave; middle identified wave for true damping; bottom, identical wave for damping neglected.

direct propagation is equivalent to negative damping in the inverse problem. Hence, noise will be unduly amplified by the inversion procedure. Obviously, this problem becomes progressively more serious as x increases.

However, when identifying excitation forces from response measurements, the inversion procedure may be more robust to noise. In Figures 3(a–d), from a signal force pulse $F(t)$ at $x = 0$, an acceleration travelling wave was generated (with $EI \approx 171$) and contaminated with noise. Then, for low damping vaues, the excitation force could be identified by inversion—including the damping effect—without excessive noise amplification (see Figures 3(a–d), with damping $\mathscr{D}' = 0{\cdot}002$). This is due to the coefficient $(k_n)^{-3}$ in equations (8). However, for higher damping values, the inversion procedure becomes very sensitive to noise if damping is included (see Figure 3(c–d), with damping $\mathscr{D}' = 0{\cdot}005$). Therefore, one must be careful when including damping effects for inverse estimations, as results are problem-dependent. If damping is neglected—and it should, for noisy signals—the results of Figure 3 suggest that the identified force might be corrected by using a suitable amplifying factor. A simple form for such factor is not readily available, although it should depend on the damping parameter, the impact distance and also probably on the pulse shape. Problems of noise amplification can sometimes be overcome by adequate filtering of the signals. This will be further discussed in Part 2 of this work.

In Figures 4(b–d) the amplitude and phase of the transfer function $G_f(x, \omega)$ have been computed from the Fourier transforms of the displacement signals at $x = 0$ and $x = 1$ m, as shown in Figure 4(a):

$$G_f(x, \omega) = Y_f(x, \omega)/Y_0(\omega). \tag{13}$$

The results in Figures 4(b–d) are shown as a function of the noise contamination, identical for both response signals (with noise levels between $0 \sim 1\%$). Once can notice that formulation (13) is very sensitive to noise, and that the frequency range where G_f is badly estimated increases with the level of contamination. Indeed, for more realistic noise levels of about 10%, estimation of parameters $\mathscr{C}$ and $\mathscr{D}'$ from G_f would be useless. Such an inverse problem is very ill-posed and should be solved differently.

3.2. REGULARIZATION METHODS

As discussed in section 1, ill-conditioning of inverse problems may be overcome by several methods. Often, noise contamination effects may be filtered out by using many approaches, including singular-value decomposition of the transformation/propagation operators [36]. Another approach is to enforce some additional physical knowledge in the inversion process—for instance, the solution domain may be known, or some analytical

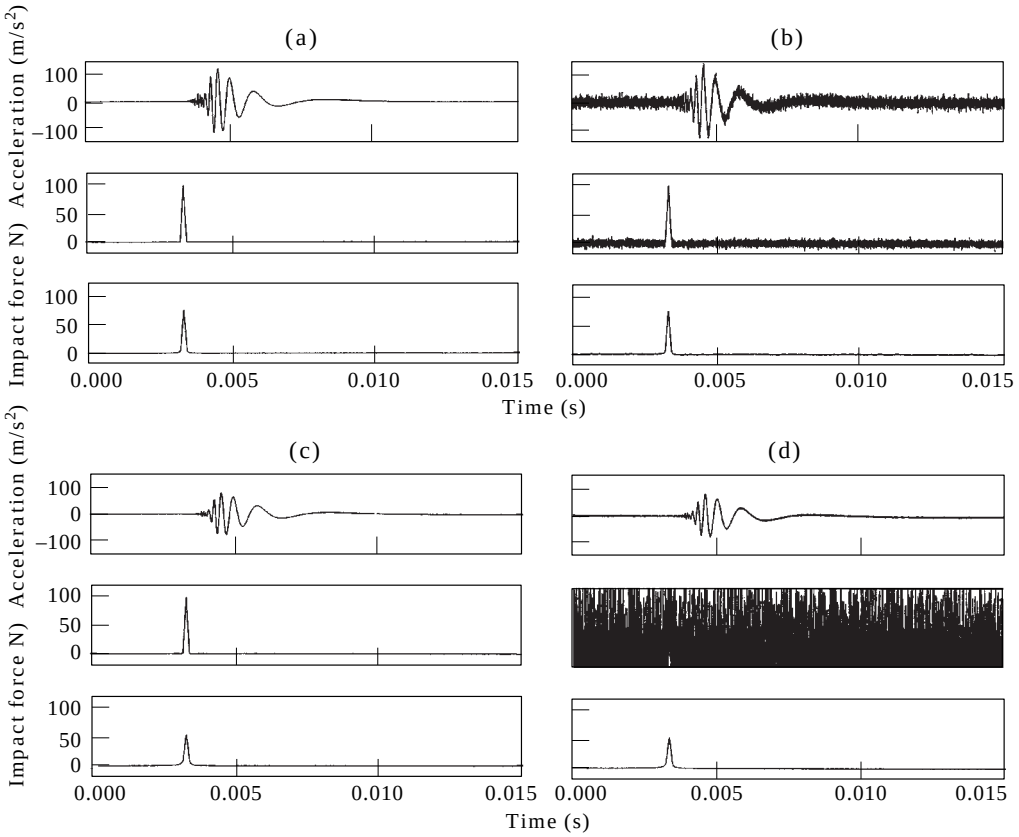

Figure 3. Remote Identification of a pulse force, from the travelling wave measured distance at $x = 1$ m. Effect of the noise contamination (wave generated with $EI \cong 171$ and $\mathscr{C} = 0{\cdot}3446$): (a) 0% noise and $\mathscr{D}' = 0{\cdot}002$; (b) 50% noise and $\mathscr{D}' = 0{\cdot}002$; (c) 0% noise and $\mathscr{D}' = 0{\cdot}005$; (d) 10% noise and $\mathscr{D}' = 0{\cdot}005$. For each part, top, middle and bottom graphs as in Figure 3.

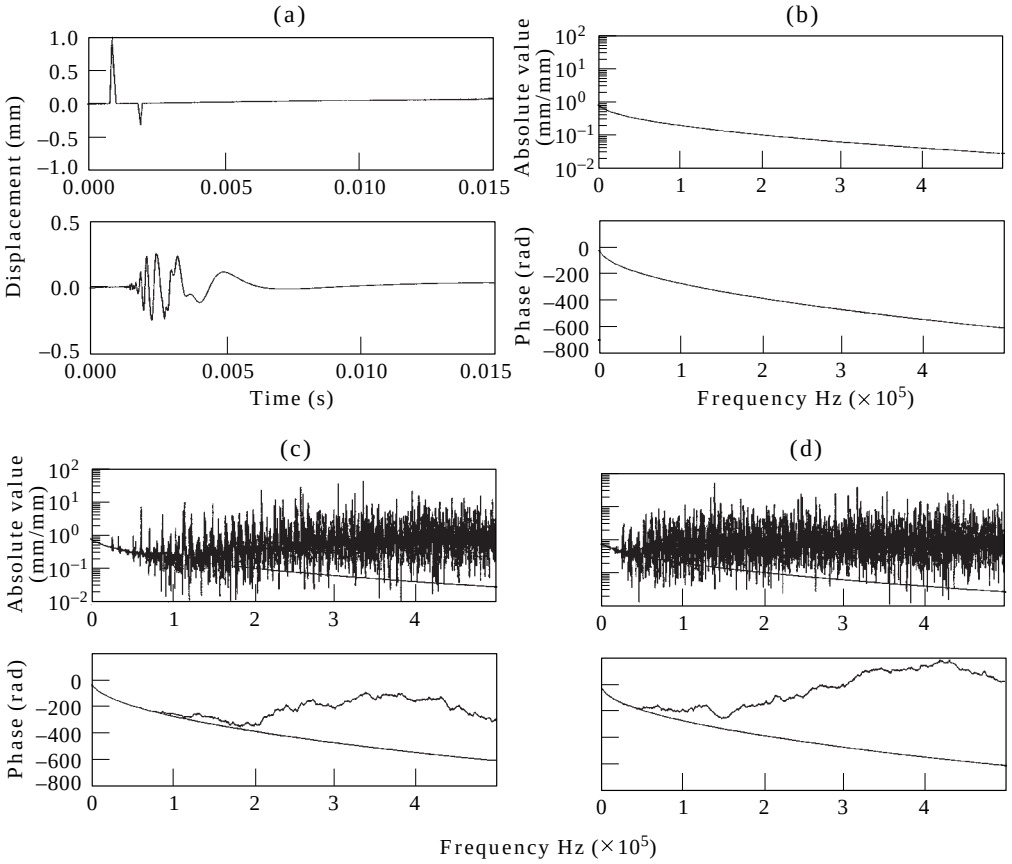

Figure 4. Estimation of the transfer function $G_f(x, \omega)$ from two wave measurements at distance $x = 1$ m, as a function of the noise contamination: (a) time-domain waves at $x = 0$, top and $x = 1$ m, bottom; (b) $G_f(x, \omega)$ with 0% noise; (c) $G_f(x, \omega)$ with 0·1% noise; (d) $G_f(x, \omega)$ with 1% noise.

form may be postulated for the solution. Then, the inversion process may be formulated as an optimization problem, with or without penalty constraints [33–35]. This approach seems well adapted to the problem discussed in section 3.1, and optimization will be formulated as follows.

Given the noisy signals $y_0(t)$ and $y_f(x, t)$, and assuming a propagation function in the form

$$G_f(x, \omega) = \mathrm{e}^{-\mathrm{i}k(\omega)x}, \qquad k(\omega) = (\mathscr{C} - \mathrm{i}\mathscr{D}')\sqrt{\omega}. \tag{14}$$

find parameters $\mathscr{C}$ and $\mathscr{D}'$ in order to minimize a suitable cost function $\varepsilon(\mathscr{C}, \mathscr{D}')$. Many functions ε may be used, such as the L_1 norms (respectively in the time and frequency-domain),

$$\varepsilon_1(\mathscr{C}, \mathscr{D}) = \sum_{t_n}^{T} |y_f(x, t_n) - \mathscr{F}^{-1}[\mathscr{F}[y_0(t_n)]G_f(x, \omega_n, \mathscr{C}, \mathscr{D})]|, \tag{15}$$

$$\varepsilon_2(\mathscr{C}, \mathscr{D}) = \sum_{\omega_n}^{\Omega} |Y_f(x, \omega_n) - Y_0(\omega_n)G_f(x, \omega_n, \mathscr{C}, \mathscr{D})|, \tag{16}$$

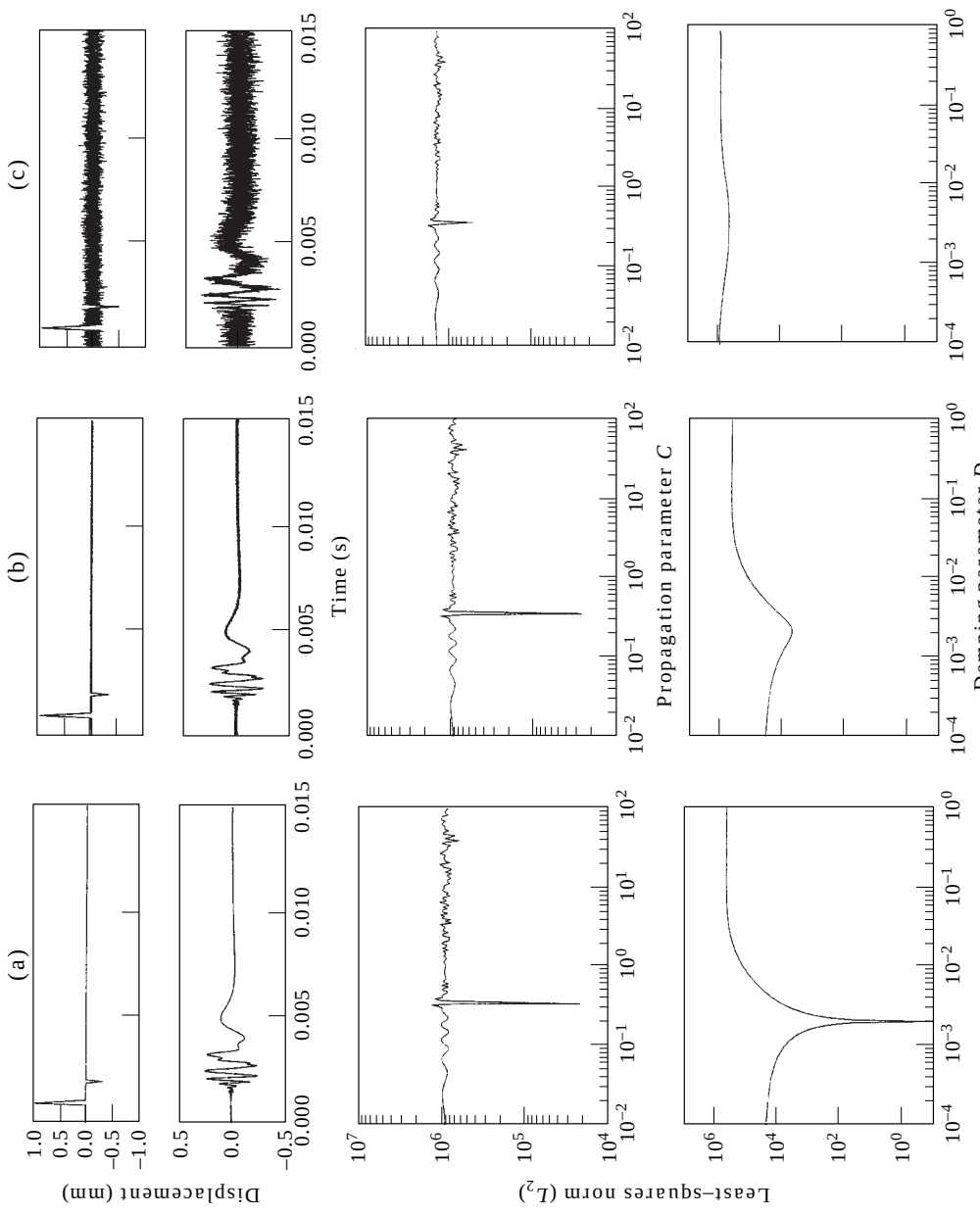

Figure 5. Error surface cuts along directions $\mathscr{C}$ and $\mathscr{D}'$, by using L_2 cost function in the frequency-domain (wave generated with $\mathscr{C} = 0{\cdot}3446$ and $\mathscr{D}' = 0{\cdot}002$; travelling distance 1 m). From top to bottom: (a) wave at location 0 m, wave at location 1 m, $\varepsilon(\mathscr{C})$ with $\mathscr{D}'$ constant, $\varepsilon(\mathscr{D}')$ with $\mathscr{C}$ constant (0% noise); (b) wave at location 0 m, wave at location 1 m, $\varepsilon(\mathscr{C})$ with $\mathscr{D}'$ constant, $\varepsilon(\mathscr{D}')$ with $\mathscr{C}$ constant (10% noise); (c) wave at location 0 m, wave at location 1 m, $\varepsilon(\mathscr{C})$ with $\mathscr{D}'$ constant, $\varepsilon(\mathscr{D}')$ with $\mathscr{C}$ constant (100% noise).

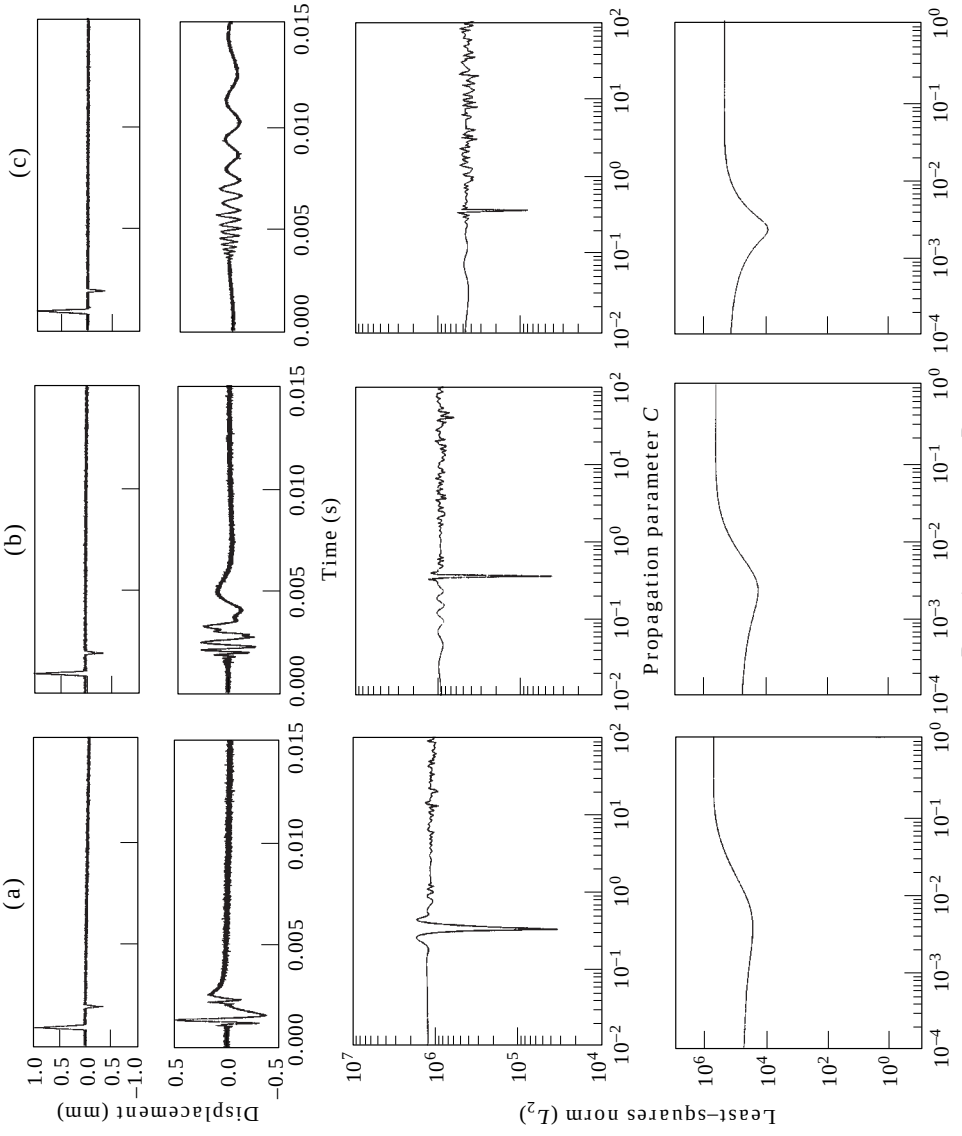

Figure 6. Error surface cuts along directions $\mathscr{C}$ and $\mathscr{D}'$, by using L_2 cost function in the frequency-domain (wave generated with $\mathscr{C} = 0{\cdot}3446$ and $\mathscr{D}' = 0{\cdot}002$; 20% noise contamination). From top to bottom: (a) wave at location 0 m, wave at location 0·3 m, $\varepsilon(\mathscr{C})$ with $\mathscr{D}'$ constant, $\varepsilon(\mathscr{D}')$ with $\mathscr{C}$ constant; (b) wave at location 0 m, wave at location 1 m, $\varepsilon(\mathscr{C})$ with $\mathscr{D}'$ constant, $\varepsilon(\mathscr{D}')$ with $\mathscr{C}$ constant; (c) wave at location 0 m, wave at location 3 m, $\varepsilon(\mathscr{C})$ with $\mathscr{D}'$ constant, $\varepsilon(\mathscr{D}')$ with $\mathscr{C}$ constant.

or the corresponding L_2 (least-squares) norms,

$$\varepsilon_3(\mathscr{C}, \mathscr{D}) = \sum_{t_n}^{T} |y_f - \mathscr{F}^{-1}[\mathscr{F}[y_0]G_f]|^2, \qquad \varepsilon_4(\mathscr{C}, \mathscr{D}) = \sum_{t_n}^{T} |Y_f - Y_0 G_f|^2, \tag{17, 18}$$

or some more exotic criteria, such as the Cauchy and hyperbolic cost functions [46, 47],

$$\varepsilon_5(\mathscr{C}, \mathscr{D}) = \sum_{t_n}^{T} \ln\{1 + |y_f - \mathscr{F}^{-1}[\mathscr{F}[y_0]G_f]|^2\}, \qquad \varepsilon_6(\mathscr{C}, \mathscr{D}) = \sum_{\omega_n}^{\Omega} \ln\{1 + |Y_f - Y_0 G_f|^2\}, \tag{19, 20}$$

$$\varepsilon_7(\mathscr{C}, \mathscr{D}) = \sum_{t_n}^{T} \ln\cosh\{y_f - \mathscr{F}^{-1}[\mathscr{F}[y_0]G_f]\}, \qquad \varepsilon_8(\mathscr{C}, \mathscr{D}) = \sum_{\omega_n}^{\Omega} \ln\cosh\{Y_f - Y_0 G_f\}. \tag{21, 22}$$

A critical appraisal of these formulations will be provided in sections 3.4 and 4.4, based on numerical simulations and experimental results.

3.3. OPTIMIZATION ALGORITHM

Solution of problem (14, 15–22) may be attempted by using a number of methods, including both deterministic and random search strategies [33]. Figures 5 and 6 show, for several noise levels and travelling distances, the change of error surface $\varepsilon(\mathscr{C}, \mathscr{D}')$ along two orthogonal directions. These functions, $\varepsilon(\mathscr{C}, 0{\cdot}002)$ and $\varepsilon(0{\cdot}3446, \mathscr{D}')$, were computed from formulation (18)—the least-squares norm (L_2). One may notice that the error functions usually display many unimportant local minima. As a result, for this type of problem,

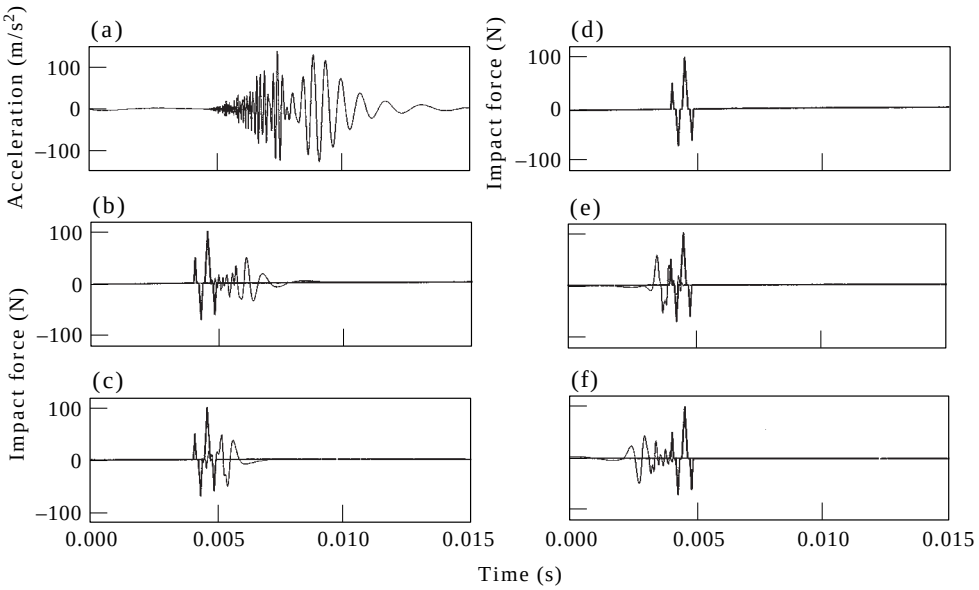

Figure 7. True impact force and force estimation, from a wave response at a travelling distance 3 m, for several impact distances in the inversion procedure (wave generated by using $EI \approx 171$, $\mathscr{C} = 0{\cdot}3446$ and $\mathscr{D}' = 0{\cdot}0005$). (a) Noisy wave at location 3 m; noise = 0%. (b)–(f) True force and identified force at distances of 2, 2·5, 3, 3·5 and 4 m, respectively.

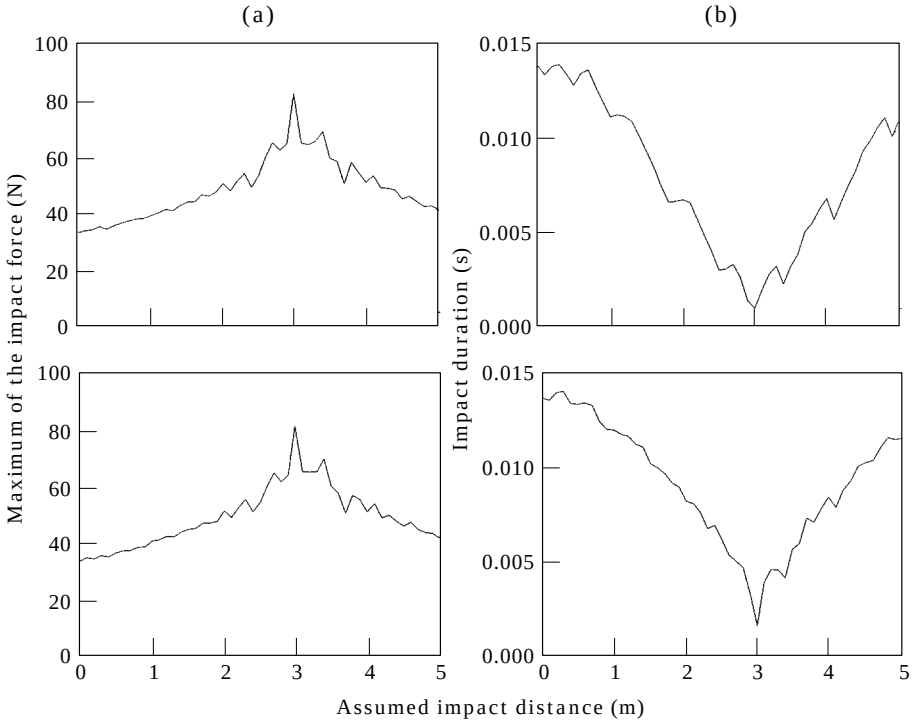

Figure 8. Error functions from the estimated impact forces, as a function of the assumed impact location (wave generated at distance 3 m, by using $EI \approx 171$, $\mathscr{C} = 0{\cdot}3446$ and $\mathscr{D}' = 0{\cdot}0005$; 0% (top) and 50% (bottom) noise contamination): (a) identification by using formulation (26); error function 1. (b) identification by using formulation (27); error function 2.

current deterministic algorithms are not well suited to search for the optimal values $\mathscr{C}_a$ and $\mathscr{D}'_a$ (e.g., the global minimum of ε). This statement is strengthened by noting that, in general, more than two pertinent parameters may exist—this would lead to extremely expensive deterministic multi-dimensional global search schemes. Hence, stochastic optimization methods are much better adapted to this problem. Here, the powerful simulated-annealing method [30, 33, 48–50] was adapted in order to allow a multi-dimensional search in a continuous space. Our implementation will now be described briefly.

In stochastic optimization methods, global optimization is achieved by occasionally allowing the iteration procedure to accept an increase in the cost function ε, in order to avoid being trapped by local minima. In simulated annealing, the optimization procedure was inspired by the slow cooling of metals during annealing, which leads to quasi-minimal energy states of the ordered media. Eventual escape from local minima is achieved by postulating a probability distribution for the possible "energy" states ε of the system—as computed from equations (15–22)—during the "cooling" process. The Boltzmann probability distribution is commonly used,

$$\text{Prob}\,(\varepsilon) = \mathrm{e}^{-\varepsilon/cT}, \tag{23}$$

where the parameter T is analogous to the current "temperature" in the cooling process and c is a suitable scaling constant. Then, higher values of the cost function ε may be allowed at any iteration, with a probability which decreases with T, allowing the process to escape from local minima. When the parameter T is high, at the beginning of the

optimization, large portions of the search space are explored in order to find the deepest valley of the "energy" surface. Later, as T decreases, only lower values of the cost function ε will be progressively allowed, in order to refine the search for the global minimum.

The "cooling" schedule used here is given as

$$T(s+1) = rT(s), \qquad T(0) = T_0, \tag{24}$$

where $s = 0, 1, 2, 3, \ldots$ and $r = 0{\cdot}9$. Relation (24) is applied after every 100 iterations at constant "temperature". In our implementation of the annealing algorithm, the search (for each variable V_i) proceeds in a random manner, inside a continuous search domain S_i, centered on the previously accepted iteration. The size of the search domain also decreases with the optimization "temperature":

$$S_i(s+1) = rS_i(s), \qquad S_i(0) = S_{i0}. \tag{25}$$

Starting values of the variables are chosen randomly inside physically plausible search domains. The iteration/cooling scheme proceeds until, for a large number of moves, no further decrease of the "energy" (cost function) is achieved. Further details can be found in the above mentioned references.

3.4. ESTIMATION OF THE WAVE-PATH PARAMETERS

Extensive numerical simulations have been performed by using formulations (15–22), for several levels of noise contamination, in order to choose better error criteria for this problem. From these tests one obtains the following conclusions: results obtained by using time-domain cost functions are similar to those obtained by using the corresponding frequency-domain functions; The Cauchy and hyperbolic cost functions do not improve results over those obtained by using the common L_1 or L_2 norm cost functions; for any cost function, and up to 100% of noise contamination (at least), the propagation constant $\mathscr{C}$ is sharply defined by the global minimum of the error surface $\varepsilon(\mathscr{C}, \mathscr{D}')$; however, when noise contamination is high, the damping parameter $\mathscr{D}'$ is not clearly defined by the global minimum of $\varepsilon(\mathscr{C}, \mathscr{D}')$.

Obviously, optimizations performed in the frequency-domain are less computer-intensive than if the corresponding time-domain cost functions are used. Therefore, from the first and second conclusions, only L_1 or L_2 frequency-domain criteria will be used for the experimental identification. To illustrate the third and fourth conclusions, Figure 5(a) shows the error surface $\varepsilon(\mathscr{C}, \mathscr{D}')$ along two orthogonal directions, as explained earlier. Here, we used the signals of Figures 1(a) and (e), after the wave travelled 1 m (with propagation parameters $\mathscr{C} = 0{\cdot}3446$ and $\mathscr{D}' = 0{\cdot}002$). Figures 5(b, c) show the corresponding information, when the response signals are contaminated with 10% and 100% noise, respectively.

Another interesting aspect is the sensitivity of the results to the travelling distance between the transducers used for the identification procedure. Figure 6 shows the change of the error surface functions (when noise contamination is 20%), for three values of the distance between transducers: 0·3, 1 and 3 m. These results show that the error minimum corresponding to the optimal propagation parameter $\mathscr{C}$ is better defined for short travelling distances, and the opposite is true for the damping parameter $\mathscr{D}'$, which is better defined when transducers are well separated.

Clearly, this aspect is better tolerated by the parameter $\mathscr{C}$. Hence, results suggest that wave-path identification should preferably be based on responses from well separated transducers—at least when signals are noisy.

3.5. ESTIMATION OF THE IMPACT EXCITATION

Two important aspects should be considered when addressing impact identification, using travelling wave measurements: the identification of the impact forces; the identification of the impact locations.

The first aspect has been discussed in section 3.1 (see Figure 3), under the assumptions that both the system parameters and the impact locations were known. In sections 3.1 to 3.4 we presented the basics of identifying the propagation parameters. Here we deal with the second aspect—the identification of the wave source locations—assuming that propagation parameters have already been extracted in an adequate manner.

A straightforward approach to this problem takes advantage of the dispersive nature of flexural waves. As shown in section 3.1, dispersive waves generated by pulse forces are such that one can impose the following constraints: the absolute value of the signal amplitude is maximum at the wave origin; the duration of the travelling wave is minimum at the wave origin; waves generated by unilateral impacts are oscillatory everywhere except at the impact location. One thus has three possible criteria for identifying the impact locations. Then, the unknown impact location may x_0 may be estimated by solving one of the optimization problems described next.

Given the (noisy) response signal $y_f(x, t)$—and assuming a propagation function in the form (14) with k_n given by formulations (9–11)—find the impact distance x_0 in order to maximize the cost function

$$\delta_1(x) = \text{Max } |F(x, t)|, \tag{26}$$

or to minimize the cost function

$$\delta_2(x) = t_c \Rightarrow |F(x, t_c)| > F_{noise}, \tag{27}$$

where t_c is the duration of the reconstructed impact force (with respect to a given noise floor level).

For unilateral impacts, the third criterion leads to minimizing negative force regions, when identifying positive pulses (or minimizing positive residuals, for negative forces). This is equivalent to minimizing the cost functions:

$$\delta_{3a}(x) = \int [F(x, t) < 0]\, \mathrm{d}t \quad \text{(for positive impact forces)},$$

$$\delta_{3b}(x) = \int [F(x, t) > 0]\, \mathrm{d}t \quad \text{(for negative impact forces)}. \tag{28}$$

In the preceding formulations, the impact force is computed as previously described:

$$F(x, t) = \mathscr{F}^{-1}[\mathscr{F}[\, y_{fn}(x, t_n)]\tilde{G}_{fn}^{-1}(x, \omega_n)]. \tag{29}$$

For unilateral impacts, these three methods are adequate. However, for most systems, impact forces are generated by two-side stops, which rules out the third method. When using the second method, a user-defined noise threshold must be provided. This is a slight inconvenience, as this method accommodates a range of threshold levels (in these tests, 1/50 of the maximum of the identified force was found adequate). In practice, both criteria (26) and (27) perform well, as will be shown in Figure 8.

Figure 7 shows several "impact forces", identified from an acceleration wave distanced 3 m from the true impact location. This wave was generated from a two-side impulsive force, by using propagation parameters $\mathscr{C} = 0{\cdot}3446$ and $\mathscr{D}' = 0{\cdot}0005$ (a realistic value of

the damping constant, for our experiments). Then, following previous conclusions, damping was neglected in the inversion procedure when using equation (29). The true force is superposed to each identification attempt, for several values of the assumed impact distance (in the range $2 \leqslant x \leqslant 4$ m). Dispersive effects on the reconstructed force are clearly shown, on both sides of the true impact location.

(a)

(b)

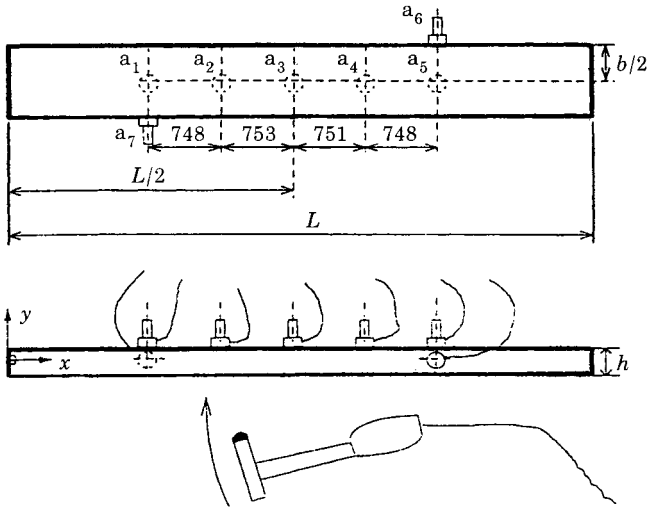

Figure 9. (a) Experimental set-up; (b) Instrumentation.

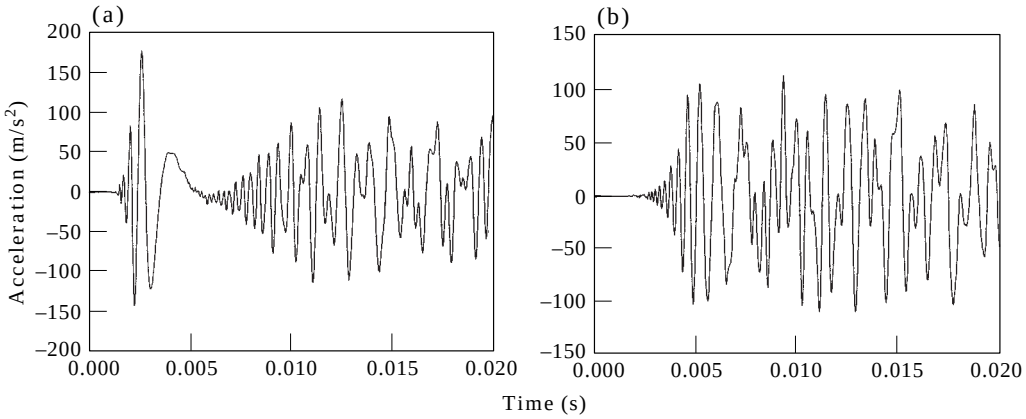

Figure 10. Typical wave generated by an impact on the beam, showing the contribution of reflected waves: (a) response of accelerometer a_3 measured wave at distance 0·753 m from impact. (b) response of accelerometer a_5; measured wave at distance 2·252 km from impact.

The practical consequences of such behaviour are illustrated in Figures 8(a, b), where the error criteria (26) and (27) are computed as a function of the assumed impact distance. Illustrative plots are presented for no-noise and 50% noise conditions (on the acceleration wave). From these results, it appears that both methods are effective and that force estimations may be achieved under quite noisy conditions (at least, for lightly damped systems). Figures 8(a, b) also display many local maxima and minima, indicating that conventional optimization methods are unsuited for this problem. Again, the stochastic algorithm described in section 3.3 proved to be adequate. Indeed, this method should be invaluable for the blind estimation of impact forces (and the corresponding force locations) on complex multi-impact problems.

4. EXPERIMENTAL PROCEDURES

4.1. TEST RIG

Figure 9(a) shows the experimental set-up, consisting on a stainless steel AISI 304 laminated beam with cross-section $50 \times 5{\cdot}9$ mm and length about 6 m. The beam is supported only at the extremities, with the larger surfaces in the vertical position, by using (almost) clamped–clamped boundary conditions. The beam supports are mounted on heavy concrete blocks. The Young's modulus of the beam is about 2×10^{11} Pascal and the mass density is about $7{\cdot}9 \times 10^3$ kg/m^3. Errors of $\pm 1\%$ were found in the cross-section dimensions along the beam and an uncertainty of $\pm 5\%$ is expected in the values of E and ρ. Then, the parameter $\mathscr{C} = [\rho A/EI]^{1/4}$ is estimated to lie between 0·332 and 0·352. Dissipative effects are very low (modal damping was less than 0·1%, for the first beam mode).

4.2. INSTRUMENTATION

Excitation was performed with an instrumented hammer Brüel and Kjaer (B&K) 8202, which has a piezoelectric force transducer B&K 8200, equipped with a hard plastic tip (impact stiffness was measured at 4×10^6 N/m). Vibratory responses were sensed by using several miniature accelerometers B&K 4375, located as shown in Figure 9(b). Impacts were always imposed along direction y, facing accelerometer a_2, on the neutral axis of the beam.

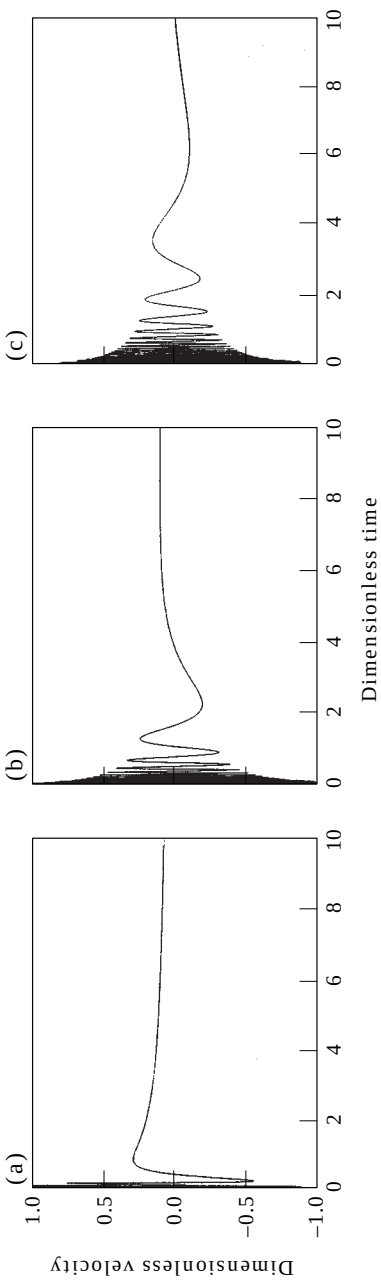

Figure 11. Theoretical response wave generated by a Dirac excitation on an infinite beam, as a function of dimensionless time ϑ and distance χ, where (a) $\chi = 2$, (b) $\chi = 6$, (c) $\chi = 10$.

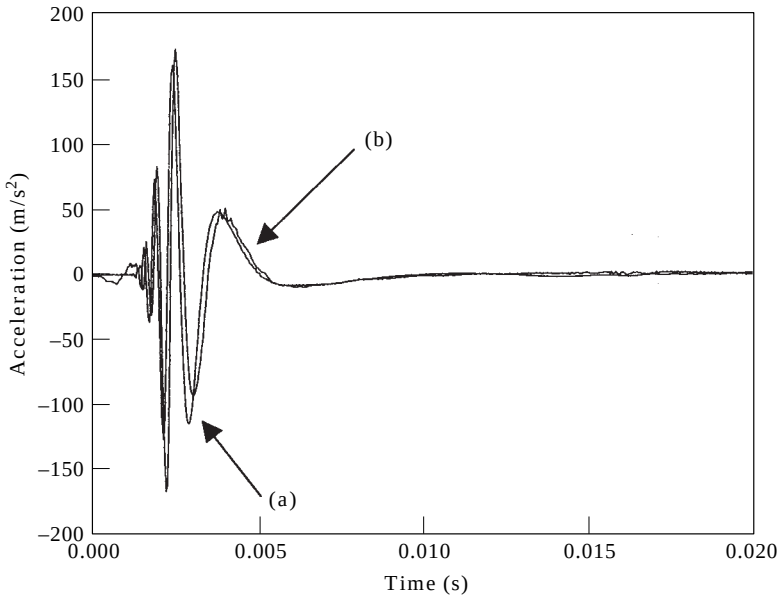

Figure 13. Two estimates of the acceleration response at locations a_3, at distance 0·753 m, with the optimal parameters $\mathscr{C}_0$ and $\mathscr{D}_0$: (a) from the measured force at location a_2; (b) from the "cleaned" acceleration at location a_5.

Accelerometers a_1 to a_5 were used to sense the "useful" waves (direction y), while accelerometers a_6 and a_7 monitored residual vibrations in the orthogonal direction. On purpose, the accelerometers used in these experiments were selected and mounted without aiming at better-than-average precision or phase matching specifications. Indeed, based on preliminary calibrations, the magnitude errors are expected within 10% and phase errors should lie within $\pm 5^\circ$. These results apply to the mounted transducers, in the frequency range 500 Hz $\sim$ 4 kHz. The non-quantified effects of accelerometers on the beam vibratory responses are assumed to be small. Data acquisition was achieved with a National Instruments (AT-MIO-16F5) 8-channel 12-bit card, using signal blocks of 0·02 s and a digitizing frequency of 25 kHz. This is consistent with the frequency range where signals displayed significant energy (up to 4 $\sim$ 5 kHz). No anti-aliasing filters were used, in order to avoid filter-induced signal distortions in the frequency range of interest. However, because of the steady signal energy decrease for increasing frequencies—and accounting for the relatively high sampling rate—aliasing effects should be negligible. Signal processing and system identification were performed with a PC-based software, which was developed by using the MATLAB computing environment.

4.3. REMOVAL OF REFLECTED WAVES

Figure 10 shows a typical wave generated by an impact on the beam at location a_2 and sensed by accelerometers a_3 and a_5. One can see that, before the lower-frequency components of the direct wave have died out, a second and further waves arrive—as the result of reflections on the boundaries. These reflected waves obviously pollute the useful signal, and will induce severe errors on the results predicted by inversion. This is one of the main problems when dealing with realistic vibro-impacting systems, where a multitude of direct and reflected waves travel simultaneously. Here, a simple approach will be

adopted to remove reflections, which is adequate if a significant part of the direct wave is available before arrival of the first reflection—such is the case for these experiments.

In Figure 10 the arrival of the first wave reflection can be clearly spotted at some time t_r, when the low-frequency "tail" of the direct wave is suddenly perturbed by the high-frequency content of the first reflection. The response $\ddot{y}(x, t)$ generated for single force spikes can then be separated into two distinct parts: $\ddot{y}_d(x, t)$ and $\ddot{y}_r(x, t)$. The reflected wave might be predicted and subtracted if the boundary conditions were perfectly known [22]. However, this is not the case for the majority of complex systems, and we will avoid such an approach. Instead, we prefer to extrapolate the direct wave beyond the arrival time t_r of the first reflection. This will be done by using the theoretical solution of the wave propagation problem in an infinite beam, when excited by a pulse excitation. Such a solution should be adequate when used after a significant time, with respect to the time-scale of the force, as shown next.

As shown in reference [51], the dimensionless wave solution to a Dirac excitation applied at instant $t = 0$ is given by

$$Y(\chi, \vartheta) = \frac{1}{\sqrt{8\pi}} \int_0^{\vartheta} \frac{\cos(\chi^2/4\vartheta) + \sin(\chi^2/4\vartheta)}{\sqrt{\vartheta}} \, \mathrm{d}\vartheta, \tag{30}$$

where the dimensionless variables are related to physical parameters through relations $\chi = x\sqrt{A/I}$ and $\vartheta = t\sqrt{AE/I\rho}$.

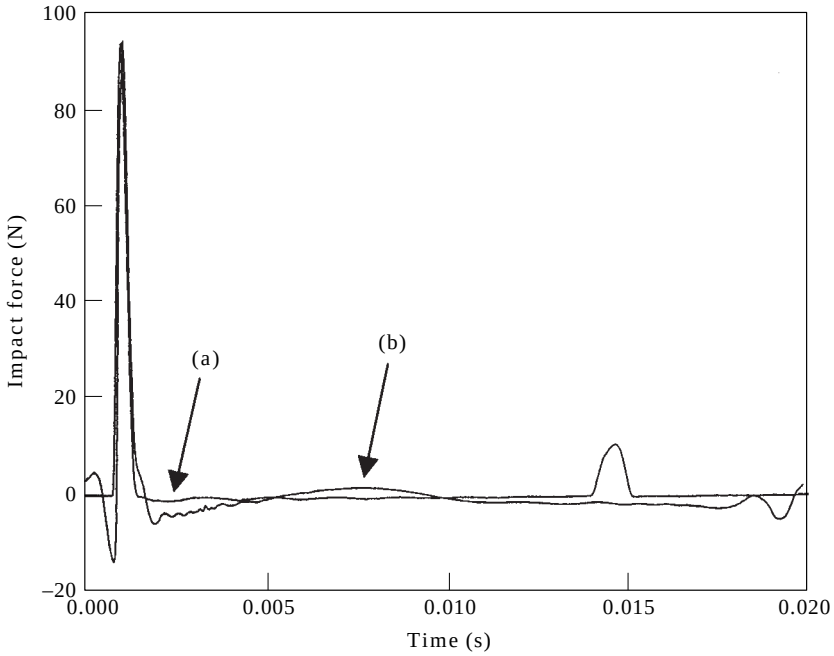

Figure 14. (a) Measured impact force; (b) estimation of the impact force, from the acceleration response at location a_3, by using the optimal parameter $\mathscr{C}_0$.

TABLE 1

Correlation coefficients of the acceleration response estimates at location a_3 for several cost functions

Correlation coefficients	Time-domain cost functions		Frequency-domain cost functions	
	Norm L_1	Norm L_2	Norm L_1	Norm L_2
Model (9)	0·71	0·70	0·66	0·70
Model (10)	0·68	0·70	0·67	0·70
Model (11)	0·69	0·70	0·67	0·70

The wave displacement formulation (30) has no closed-form solution. However, solutions for the velocity and acceleration waves are quite convenient:

$$\dot{Y}(\chi, \vartheta) = \frac{1}{\sqrt{8\pi}} \frac{\cos(\chi^2/4\vartheta) + \sin(\chi^2/4\vartheta)}{\sqrt{\vartheta}}, \tag{31}$$

$$\ddot{Y}(\chi, \vartheta) = \frac{1}{8\sqrt{2\pi}\vartheta^{2\cdot5}} \left[(\chi^2 - 2\vartheta) \sin\left(\frac{\chi^2}{4\vartheta}\right) - (\chi^2 + 2\vartheta) \cos\left(\frac{\chi^2}{4\vartheta}\right) \right]. \tag{32}$$

Figure 11 shows the velocity wave (31) as a function of dimensionless time ϑ, for three dimensionless distances χ. One may notice the very high frequency content of the wave, which is due to the frequency spectrum of a Dirac excitation, as well as to the properties of the Bernoulli–Euler beam model. This aspect is even more noticeable in the acceleration wave (32). However, such high-frequency content is not realistic, because (a) the excitation energy is bounded at high-frequency, and (b) the beam really acts as a filter for very high frequencies (a result which stems from the Timoshenko theory). More interesting for our purpose is the lower-frequency response, later in time, with an asymptotic decrease as $\vartheta^{-0\cdot5}$ (for velocity) or as $\vartheta^{-1\cdot5}$ (for acceleration). In this frequency range, the Bernoulli–Euler beam model is quite reliable and can be used for extrapolation of the experimental flexural waves.

TABLE 2

True and estimated impact distances for several optimization criteria

True impact distance	2·25 m
Using method (26)	2·25 m
Using method (27)	2·24 m
Using method (28)	2·25 m

From formulation (32) and after some algebra, it can be shown that the truncated part of the experimental accelerations (after time t_r) should be replaced by

$$\ddot{y}(x, t > t_r) =$$

$$\ddot{y}(x, t_r)\,\frac{\dfrac{1}{(t-t_0)^{2\cdot5}}\left\{[a-2b(t-t_0)]\sin\left(\dfrac{a}{4b(t-t_0)}\right)-[a+2b(t-t_0)]\cos\left(\dfrac{a}{4b(t-t_0)}\right)\right\}}{\dfrac{1}{(t_r-t_0)^{2\cdot5}}\left\{[a-2b(t_r-t_0)]\sin\left(\dfrac{a}{4b(t_r-t_0)}\right)-[a+2b(t_r-t_0)]\cos\left(\dfrac{a}{4b(t_r-t_0)}\right)\right\}}, \tag{33}$$

where the parameters a, b and the impact time t_0 are computed by minimizing the difference between the original wave (with reflections) and formulation (33).

Again, the optimization algorithm described in section 3.3 was found adequate to compute a, b and t_0, by using physically plausible starting-values for these parameters. Figure 12 shows the original waves from accelerometers a_3 and a_5, as well as the corresponding "cleaned" waves. For multiple impact forces, or when boundaries are very close to the motion transducers, the described extrapolation procedure is not adequate. Indeed, a significant part of the direct wave may not be available before arrival of the first reflection. Also, the arrival time t_r can be very difficult to spot. To deal with such difficult conditions, a more powerful wave separation method will be presented in Part 2.

4.4. ESTIMATION OF THE WAVE-PATH PARAMETERS

The techniques previously described were used to identify the propagation parameters of the system, from a pair of "cleaned" acceleration waves $\ddot{y}_3(x, t)$ and $\ddot{y}_5(x, t)$. The adequacy of the propagation models (9–11) was asserted, as well as the performance of the cost functions (15–18). Figure 13 illustrates the results obtained by using model (11) and the quadratic error function (L_2), in the frequency-domain.

Here, after optimization, the identified parameters $\mathscr{C}_a$ and $\mathscr{D}'_a$ were used to deduce two separate estimates of the response at location a_3: (1) the travelling wave inferred from the measured force at location a_2 (by using equations (8) and (11)), and (2) the travelling wave inferred from the "cleaned" acceleration wave at location a_5 (by using equations (6) and (11)). Interestingly, all results were satisfactory, and no significant differences were found between any of the propagation models and cost functions. This is illustrated by Table 1, showing the correlation coefficients of the wave estimates of Figure 13, for each of the computed cases:

From these results, it is arguable if more complex propagation models such as equations (9) or (10) deserve the trouble—at least for lightly damped systems not subjected to severe axial stresses. Concerning the error models, results from quadratic criteria appear slightly more consistent. More important, because time-domain error functions lead to heavier computations, the frequency-domain criteria should be preferred. The average identified parameters—$\mathscr{C} = 0{\cdot}343$ ($\pm 0{\cdot}04\%$) and $\mathscr{D}' = 0{\cdot}00046$ ($\pm 27\%$)—show that the expected theoretical value of the propagation coefficient ($0{\cdot}332 < \mathscr{C} < 0{\cdot}352$, see section 4.1) was quite precise. Also, as pointed out earlier, damping effects are very low for this steel beam.

4.5. ESTIMATION OF THE IMPACT EXCITATION

Identification of the impact force was performed by using the farthest wave measurement available—e.g., the "cleaned" acceleration $\ddot{y}_5(x, t)$, at an exact distance of

2·252 m from the impact location. Then, blind estimation of the excitation (force and location) was achieved through equation (29), by using the propagation parameter $\mathscr{C}$ previously identified (damping was neglected in the inversion). Because the excitation force is a unilateral pulse, all criteria (26–28) could be used to estimate the impact distance. Figure 14 shows a typical result, obtained by using the maximum amplitude criterion (26). Here, the measured force (the one with a small bump at 0·0145 s) is compared with the identified one, with an excellent agreement (the correlation coefficient between these plots is 0·92). However, the results obtained by using the other criteria are almost indistinguishable. Indeed, the optimal impact distances obtained by using the three methods described in section 3.5 lead to almost identical results, as shown in Table 2.

5. CONCLUSIONS

In this paper we have presented techniques to deal with the experimental identification of pulse excitations, using remote measurements of the flexural waves. Several aspects have been addressed; namely, (1) the identification of wave-path parameters; (2) the identification of impact forces; and (3) the identification of impact locations. The performance of these techniques was asserted through systematic numerical simulations, as well as a number of simple experiments. From this work, the following conclusions may be drawn.

Inverse problems which are ill-conditioned—and therefore very sensitive to noise contamination—may be tackled effectively by using optimization techniques instead of direct inversion. Several formulations were tested for the optimizing cost functions, with overall good results. For practical reasons (computational efficiency), frequency-domain cost functions should be used when identifying the wave-path parameters.

Stochastic optimization techniques are better adapted to these problems, because error functions display many local maxima and minima. Simulated annealing, when adapted for multi-dimensional search in a continuous space, performed well for both the wave-path and impact location identifications.

It was found that, for the problem of concern here, common Bernoulli–Euler beam theory is adequate for modelling wave propagation. Several damping models were tested (in the dispersion equation). No significant differences were found, in practice, for low-damped systems such as the one used in our tests.

On the other hand, it appears that identification of the propagation parameters may be often skipped, because (a) the experimentally identified propagation constant was well predicted by theory, and (b) under noisy conditions, inversions should be performed by neglecting damping effects.

Experiments suggest that transducers with excessive precision of phase matching are not required to achieve acceptable identification results, at least for the basic problem addressed here.

A simple technique was developed to suppress wave-reflections from the direct waves. Although effective, such a technique applies only to very simple impact problems, and is not adequate for realistic conditions, when many waves travel simultaneously. This fundamental problem will be addressed elsewhere.

In this paper, we were mostly concerned about identification tools and the feasibility of this project. The basic results presented here are quite encouraging. They suggest that remote impact-force identification, for more complex systems, is not a hopeless task—at least, provided that damping effects (how quickly the system forgets its history) are not too significant.

ACKNOWLEDGMENTS

The experiments presented in this paper were performed with the valuable assistance of Alvaro Anastácio and Marco António Vento, from the Applied Dynamics Laboratory, Instituto Tecnológico e Nuclear (ITN/ADL, Sacavém, Portugal). The authors also thank the reviewers for their thorough comments, which helped to clarify several aspects in this paper.

REFERENCES

1. R. Rogers and R. Pick 1997 *Nuclear Engineering and Design* **44**, 247–253. Factors associated with support forces due to heat exchanger tube vibration contact.
2. T. Frick, T. Sobek and R. Reavis 1984 *Symposium on Flow-Induced Vibration*, *ASME Winter Annual Meeting*, *New Orleans*, *LA*. Overview on the development and implementation of methodologies to compute vibration and wear of steam generator tubes.
3. M. Rao, G. Gupta, F. Eisinger, H. Hibbitt and D. Steininger 1987 *International Conference on Flow-Induced Vibrations*, *Bowness-on-Windermere*, *U.K*. Computer modelling of vibration and wear of multispan tubes with clearances at supports.
4. F. Axisa, J. Antunes and B. Villard 1988 *Journal of Pressure Vessel Technology*, *ASME* **110**, 7–14. Overview of numerical methods for predicting flow-induced vibrations.
5. N. Fisher, M. Olesen, R. Rogers and P. Ko 1988 *International Symposium on Flow-Induced Vibration and Noise*, *ASME Winter Annual Meeting*, *Chicago*, *IL*. Simulation of tube-to-support dynamic interaction in heat exchanger equipment.
6. N. Mahutov, T. Fesenko and S. Kaplunov 1989 *International Conference on Engineering Aero-Hydroelasticity*, *Prague*, *Czechoslovakia*. Dynamics of systems in a liquid flow and structure durability.
7. J. Antunes, F. Axisa, B. Beaufils and D. Guilbaud 1990 *Journal of Fluids and Structures* **4**, 287–304. Coulomb friction modelling in numerical simulations of vibration and wear work rate of multi-span heat-exchangers.
8. F. Axisa, J. Antunes and B. Villard 1990 *Journal of Fluids and Structures* **4**, 321–341. Random excitation of heat-exchanger tubes by cross-flow.
9. E. De Langre, B. Beaufils and J. Antunes 1991 *International Conference on Flow-Induced Vibrations*, *Brighton*, *U.K.*, *Proceedings of the Institute of Mechanical Engineers*, 253–262. The numerical prediction of vibrations in tube bundles induced cross-flow turbulence.
10. A. Fricker 1991 *International Conference on Flow-Induced Vibrations*, *Brighton*, *U.K.*, *Proceedings of the Institute of Mechanical Engineers*, 129–137. Vibro-impact behaviour of fluid-elastically unstable heat exchanger tubes with support clearances.
11. J. Antunes, E. De Langre, M. Vento and F. Axisa 1992a *Symposium on Flow-Induced Vibration and Noise*, *Anaheim*, *CA*, *ASME* **PVP-242**, 135–150. A theoretical model for the vibro-impact motion of tubes under fluidelastic instability.
12. E. De Langre, C. Hadj-Sadok and B. Beaufils 1992 *Symposium on Flow-Induced Vibration and Noise*, *Anaheim*, *CA*, *ASME* **PVP-242,** 107–131. Nonlinear vibrations induced by fluidelastic forces in tube bundles.
13. F. Axisa, A. Desseaux and R. G. Gibert 1984 *Symposium on Flow-Induced Vibration*, *ASME Winter Annual Meeting*, *New Orleans*, *LA*. Experimental study of the tube/support impact forces in multi-span pwr steam generator tubes.
14. S. S. Chen, J. Jendrzejczyk and M. Wamsganss 1984 *Symposium on Flow-Induced Vibration*, *ASME Winter Annual Meeting*, *New Orleans*, *LA*. Dynamics of tubes in fluid with tube-baffle interaction.
15. J. Cha, M. Wamsganss and J. Jendrzejczyk 1986 *ASME Pressure Vessel and Piping Conference*, *Chicago*, *IL*. Experimental study on impact/fretting wear in heat exchanger tubes.
16. K. Haslinger, M. Martin and D. Steininger 1987 *International Conference on Flow-Induced Vibrations*, *Bowness-on-Windermere*, *U.K*. Pressurised water reactor steam generator tube wear prediction utilising experimental techniques.
17. J. Antunes, F. Axisa and M. Vento 1992b *ASME Journal of Pressure Vessel Technology* **114**, 23–32. Experiments on tube/support interaction with feedback-controlled instability.
18. F. Axisa and P. Izquierdo 1992 *Symposium on Flow-Induced Vibration and Noise*, *Anaheim*, *CA*, *ASME* **PVP-242,** 281–300. Experiments on vibro-impact dynamics of loosely supported tubes under harmonic excitation.

19. M. A. Vento, J. Antunes and F. Axisa 1992 *Symposium on Flow-Induced Vibration and Noise*, *Anaheim*, *CA*, *ASME* **PVP-242**, 151–166. Tube/support interaction under simulated fluid-elastic instability: two-dimensional experiments and computations of the nonlinear responses of a straight tube.
20. G. S. Whiston 1984 *Journal of Sound and Vibration* **97**, 35–51. Remote impact analysis by use of propagated acceleration signals: I—theoretical methods.
21. R. W. Jordan and G. S. Whiston 1984 *Journal of Sound and Vibration* **97**, 53–63. Remote impact analysis by use of propagated acceleration signals: II—comparison between theory and experiments.
22. J. Doyle 1989 *Wave Propagation in Structures*: *An FFT-Based Spectral Analysis Methodology*. New York: Springer-Verlag.
23. S. Q. Lin and C. N. Bapat 1992 *Journal of Sound and Vibration* **157**, 485–513. Estimation of clearances and impact forces using vibroimpact response: sinusoidal excitation.
24. S. Q. Lin and C. N. Bapat 1993a *Journal of Sound and Vibration* **163**, 407–421. Estimation of clearances and impact forces using vibroimpact response: random excitation.
25. S. Q. Lin and C. N. Bapat 1993b *Journal of Sound and Vibration* **163**, 423–428. Extension of clearance and impact force estimation approaches to a beam–stop system.
26. H. R. Busby and D. M. Trujillo 1987 *Computers and Structures* **25**, 109–117. Solution of an inverse dynamics problem using an eigenvalue reduction technique.
27. E. Wu and J. C. Yeh 1994 *A.I.A.A. Journal* **32**, 2433–2439. Identification of impact forces at multiple locations on laminated plates.
28. J. T. Kim and R. H. Lyon 1992 *Mechanical Systems and Signal Processing* **6**, 1–15. Cepstral analysis as a tool for robust processing, deverberation and detection of transients.
29. W. Jeffrey and R. Rosner 1986a *The Astrophysical Journal* **310**, 463–472. On strategies for inverting remote sensing data.
30. W. Jeffrey and R. Rosner 1986b *The Astrophysical Journal* **310**, 473–481. Optimisation algorithms: simulated annealing and neural network processing.
31. V. Dimri 1992 *Deconvolution and Inverse Theory*: *Application to Geophysical Problems*. Amsterdam: Elsevier.
32. R. L. Parker 1994 *Geophysical Inverse Theory*. Princeton, NJ: Princeton University Press.
33. W. H. Press, A. A. Teukolsky, W. T. Vetterling and B. P. Flannery 1992 *Numerical Recipes*: *The Art of Scientific Computing*. Cambridge: Cambridge University Press.
34. C. W. Groetch 1993 *Inverse Problems in the Mathematical Sciences*. Wiesbaden: Vieweg & Sohn.
35. P. C. Hansen 1994 *Numerical Algorithms* **6**, 1–35. Regularisation tools.
36. J. Antunes, M. Paulino and Ph. Piteau 1998 *Journal of Sound and Vibration* (in press). Remote identification of impact forces on loosely supported tubes: Part 2—complex vibro-impact motions.
37. P. M. Morse and K. U. Ingard 1968 *Theoretical Acoustics*. Princeton, NJ: Princeton University Press.
38. M. C. Junger and D. Feit 1986 *Sound*, *Structures and their Interaction*. Cambridge, MA: M.I.T. Press.
39. R. H. Scanlan 1970 *Journal of Sound and Vibration* **13**, 499–509. Linear damping models and causality in vibrations.
40. V. I. Babitsky and V. L. Krupenin 1985 *Oscillations in Strongly Non-linear Systems*. Moscow: Nauka.
41. V. L. Krupenin and A. M. Veprik 1996 2*nd European Nonlinear Oscillation Conference*, *Prague*, *Czechoslovakia*. Vibroconductors equipped with impact elements and distributed vibroimpact systems.
42. E. C. Titchmarsh 1973 *Introduction to the Theory of Fourier Integrals*. New York: Oxford.
43. I. N. Sneddon 1995 *Fourier Transforms*. New York: Dover.
44. A. V. Oppenheim and R. W. Schafer 1989 *Discrete-time Signal Processing*. London: Prentice-Hall International.
45. J. G. Proakis, C. M. Rader, F. Ling and C. L. Nikias 1992 *Advanced Digital Signal Processing*. New York: MacMillan Publishing Company.
46. E. Crase, A. Pica, M. Noble, J. McDonald and A. Tarantola 1990 *Geophysics* **55**, 527–538. Robust elastic nonlinear inversion: application to real data.
47. S. D. Rajan 1992 *Journal of the Acoustical Society of America* **91**, 3228–3241. Waveform inversion for the geoacoustic parameters of the ocean bottom.

48. N. METROPOLIS, A. ROSENBLUTH, M. ROSENBLUTH, A. TELLER and E. TELLER 1953 *Journal of Chemical Physics* **21**, 1087–1092. Equations of state calculations by fast computing machines.
49. S. KIRKPATRICK 1984 *Journal of Statistical Physics* **34**, 975–986. Optimisation by simulated annealing: quantitative studies.
50. J. F. SMITH and S. FINETTE 1993 *Journal of the Acoustical Society of America* **94**, 2315–2325. Simulated annealing as a method of deconvolution for acoustic transients measured on a vertical array.
51. R. J. GIBERT 1988 *Vibrations des Structures*: *Interaction avec les Fluides*; *Sources d'Excitation Aléatoires*. Paris: Eyrolles.

APPENDIX: NOMENCLATURE

A	area of the beam cross-section
C_n	wave amplitude parameters
c_n	phase speed of the waves
$\mathscr{C}$	frequency parameter of k_n
$\mathscr{D}, \mathscr{D}'$	damping parameter of k_n
E	Young's modulus of the beam
$F_y(t)$	external force
F_n	spectral coefficients of the external force
$\mathscr{F}, \mathscr{F}^{-1}$	direct and inverse Fourier transforms
$G(x, \omega_n)$	wave-to-wave transfer function
$\tilde{G}(x, \omega_n)$	force-to-wave transfer function
I	moment of inertia of the cross-section
$k_n = F(\omega_n)$	dispersion relation of the waves
N	axial tension of the beam
r	"cooling" factor in simulated annealing
s	"cooling" step in simulated annealing
S_i	search domain for variable i
t	time
t_r	arrival time of the first wave reflection
T	"temperature" in simulated annealing
x	location along the beam
$y(x, t)$	flexural beam response
y_b	backward going wave
y_f	forward going wave
Y_n	spectral coefficients of the wave
$y(\chi, \vartheta)$	dimensionless beam response
ε_m, δ_n	optimisation cost functions
ρ	mass density of the beam
η	viscosity coefficient
ω_n	circular frequency
χ	dimensionless distance
ϑ	dimensionless time